Influence of InAs, AlAs δ layers on the optical, electronic, and thermal characteristics of strain-compensated GaInAs/AlInAs quantum-cascade lasers

Miriam S. Vitiello[a)]
CNR-INFM Regional Laboratory LIT^3 and Dipartimento Interateneo di Fisica "M. Merlin," Università degli Studi di Bari, Via Amendola 173, 70126 Bari, Italy

Tobias Gresch[b)]
Institute of Physics, University of Neuchâtel, CH-2000 Neuchâtel, Switzerland

Antonia Lops, Vincenzo Spagnolo, and Gaetano Scamarcio[c)]
CNR-INFM Regional Laboratory LIT^3 and Dipartimento Interateneo di Fisica "M. Merlin," Università e Politecnico di Bari, Via Amendola 173, 70126 Bari, Italy

Nicolas Hoyler, Marcella Giovannini, and Jérôme Faist[b)]
Institute of Physics, University of Neuchâtel, CH-2000 Neuchâtel, Switzerland

(Received 9 July 2007; accepted 20 September 2007; published online 17 October 2007)

We extracted the electronic temperatures, the thermal resistance (R_L=11.5 K/W), the cross-plane thermal conductivity [$k_\perp$=2.0±0.1 W/(K m)], and the thermal boundary resistance [TBR=$(4.1-9.3)\times10^{-10}$ K/W m^2] in strain-compensated $Ga_{0.609}In_{0.391}As/AlIn_{0.546}As_{0.454}$ quantum-cascade lasers operating at 4.78 μm in continuous wave up to 15 °C and in pulsed mode up to 40 °C. Submonolayer thick InAs and AlAs δ layers are included in the active region to increase the conduction band discontinuity. We found that potential interface broadening caused by the insertion of these δ layers allows for a 43% improvement of the thermal conductivity with respect to conventional lattice-matched GaInAs/AlInAs heterostructures. © *2007 American Institute of Physics*. [DOI: 10.1063/1.2798061]

Quantum-cascade lasers (QCLs) are unipolar semiconductor devices based on intersubband emission and a small and robust cavity design. This makes these laser sources potential for applications in trace-gas sensing, medical diagnostic, and free-space optical communications. While very high-power, pulsed operation has been recently demonstrated at heat sink temperatures as high as $T_H\sim400$ K, in the range of 3.8–9.5 μm,[1,2] continuous wave (cw) performance at $T_H>250$ K has been limited for several years due to the high device thermal resistance (R_L) that generates strong self-heating effects and potentially destructive thermally induced stresses.[3]

Since the demonstration of cw operation in GaInAs/AlInAs QCLs,[4] many efforts to improve cw temperature performance of QCLs in the range of 3–5 μm, where strained GaInAs-based materials are necessary, have been done, although the GaInAs/AlInAs material challenges become extreme with compressive and tensile mismatch values >1.4%. Improved device designs and heat sinking, including the use of thick electroplated Au on top of the waveguide,[1] epilayer-down mounting,[5] and buried heterostructures[4] have been proposed. However, although significant advances have been obtained, still high values of R_L in QCLs have been reported[6,7] due to the large interface density in the designed active regions. In fact, as predicted theoretically[8] and assessed experimentally,[7] the interface thermal resistivity in QCLs can be much larger than the resistivity of the composing materials. As a result, the active region cross-plane thermal resistivity can reach values more than one order of magnitude larger than the weighted average of the bulk values of the well and barrier materials.[9,10]

As a possible solution to reduce the interface resistivity, we propose GaInAs/AlInAs QCLs grown with smoother interfaces realized by means of interface broadening. In this letter, we report an experimental study focused on the analysis of the optical, electronic, and thermal properties of strain-compensated GaInAs/AlInAs QCLs, realized with the above procedure and operating at a wavelength of 4.78 μm.

The investigated structure was grown by molecular beam epitaxy (MBE) and is based on a variable-strain design where the injection and active regions are grown with 0.53% compressive strain in the $In_{0.609}Ga_{0.391}As$ wells and 0.47% tensile strain in the $Al_{0.546}In_{0.454}As$ barriers. In the active region, where the electrons are close to the conduction band edge, the effective conduction band discontinuity (ΔE_C) is further increased by adding submonolayer thick spikes of AlAs in the barriers and InAs in the wells. The 25 periods of injection and active region pairs have been grown on a slightly doped [[Si]=$n=(1-4)\times10^{17}$ cm^{-3}] InP substrate and are embedded between 200 and 300 nm thick layers of lattice-matched GaInAs ([Si]=$n=4\times10^{16}$ cm^{-3}) for a better confinement of the optical mode. The growth temperature was 520 °C for the cladding layers and 500 °C for the active region, respectively. In diffusion is known to cause interdiffusion of InAs δ layers in InGaAs.[11] Similarly, we assume that In diffusion leads to the InAs/InGaAs and AlAs/InAlAs interface broadening. Accordingly, the conduction band structure of Fig. 1(a) has been calculated by assuming an interface broadening of 3 Å. According to x-ray diffraction

a)Electronic mail: vitiello@fisica.uniba.it
b)Present address: Institute for Quantum Electronics, ETH Zürich, Wolfgang-Pauli-Str. 16, 8093 Zürich, Switzerland.
c)Electronic mail: scamarcio@fisica.uniba.it

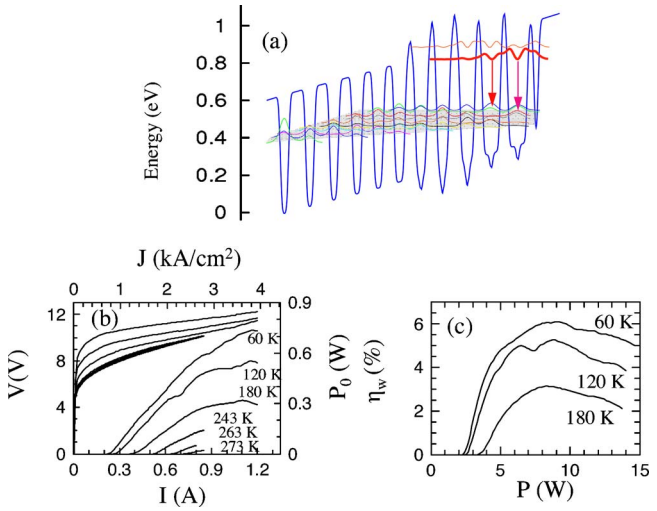

FIG. 1. (Color online) (a) Conduction band structure of one period of the active region calculated using a self-consistent Schrödinger-Poisson solver at an applied field of 78 kV/cm and assuming an interface broadening of 3 Å. The layer thicknesses in Å, starting from the injection barrier are *46*,10,*14*,[20,**2**,21],(*7*,**2**,*7*),[19,2,18],(*8*,*2*,*7*),[13,**2**,2,**2**,13], (*9*,**2**,2,**2**,*2*), [11,**2**,2,**2**,10], (*7*,**2**,2,**2**,*8*), [12,**2**,12], (*10*,**2**,*10*), 24, *23*, 22,*25*,21,*30*,20,*33*,19,*37*,18, where the underlined layers are doped so that the sheet carrier density per period is $n_s=9\times10^{10}$ cm^{-2}. The $Al_{0.546}In_{0.454}As$ layers are reported in italic, the AlAs layers in italic and bold, and the InAs layers in bold. Composite barriers and wells are further emphasized by parentheses and brackets, respectively. The shaded area represents the lowest energy miniband. The wavefunction square modulus of the upper laser levels is reported in bold. (b) Voltage and emitted power as a function of current measured at different heat sink temperatures under device continuous wave operation. (c) Wall-plug efficiency plotted as a function of the total power in the device at the heat sink temperatures marked on the figure.

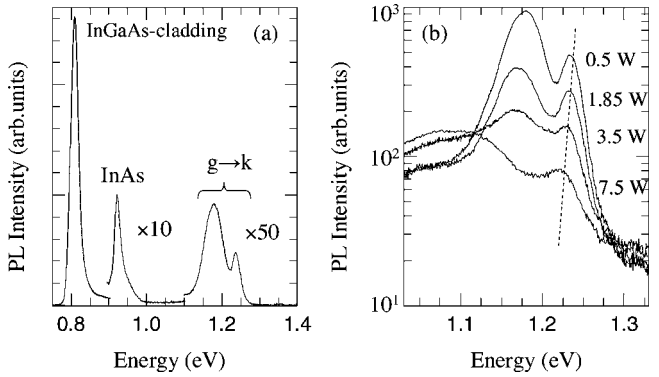

FIG. 2. (a) PL spectra collected at $V=0$ V. The heat sink temperature is $T_H=60$ K. The high energy PL bands peaked at 0.92 eV and 1.18–1.24 eV are multiplied by factors of 10 and 50, respectively. (b) Representative PL spectra measured at different dissipated powers (P) at $T_H=60$ K. The dashed line indicates the redshift of the high energy PL bands with P.

measurements, the active region period is 2.5% thicker than expected. This explains why laser emission occurs at $\lambda=4.8$ μm and slightly departs from the designed value (4.6 μm). On top of the MBE grown layers, a 2 μm thick InP ([Si]$=n=1\times10^{17}$ cm^{-3}) cladding layer and two lattice-matched GaInAs contact layers (400 nm [Si]$=n=7\times10^{17}$ cm^{-3} and 50 nm [Si]$=n>1\times10^{19}$ cm^{-3}) have been grown by metallorganic vapor phase epitaxy.

Ridge waveguides of 8–13 μm width have been defined by standard photolithography via an HNO_3:HBr:H_2O (1:1:10) based wet-etching procedure. A 300 nm thick SiO_2 layer has been deposited for electrical insulation and windows are opened on top of the waveguide ridges in order to electrically contact the structure. Top and back (Ge:12 nm/Au:27 nm/Ti:10 nm/Au:200 nm) ohmic contacts have been evaporated after lapping the sample down to 150 μm thickness. A 5 μm thick gold layer was deposited on the top contact by using a commercial gold-plating solution. Finally, a high reflectivity coating (Al_2O_3/Au/Al_2O_3) has been evaporated on the back facet. Laser bars of 3 mm long were then cleaved and indium soldered on copper mounts.

Laser action at 4.78 μm has been observed in both pulsed and cw operation. In pulsed mode, with 1% duty cycle, the threshold current densities (J_{th}) are 1.12 kA cm^{-2} at −30 °C and 1.65 kA cm^{-2} at 30 °C and the characteristic temperature is $T_0=171$ K. At −30 °C, a maximum average power of 480 mW has been measured by using a 50% duty cycle. This value drops to 213 mW at 30 °C.

Figure 1(b) shows the current-voltage (I-V) and light-current (L-I) characteristics in cw measured as a function of selected T_H for the investigated device. Laser action has been observed up to 288 K with $J_{th}=1.81$ kA cm^{-2} and $T_0=88$ K. The maximum output power is $P_o=150$ mW at $T_H=-30$ °C. A maximum value of $P_o=200$ mW has been observed with longer (4.11 mm) devices. The wall-plug efficiency (η_w) values extracted from the ratio P_o/P are reported in Fig. 1(c) as a function of the total electrical power (P). A maximum value $\eta_w\sim6\%$ has been measured at $T_H=60$ K.

Band-to-band photoluminescence (PL) experiments were carried out during cw operation. The samples were mounted on the cold finger of a helium-flow microcryostat. The heat sink temperature was kept at 60 K and controlled by a Si diode mounted close to the device. The 647 nm line of a Kr^+ laser was focused to a 2.5 μm spot onto the device front facet by fixing the optical power density at 10^3 W/cm^2. The PL signal was dispersed using a 0.46 m monochromator and detected with a GaInAs diode array cooled to 240 K. Figure 2(a) shows the PL spectrum collected at device off. Three main structures can be observed: (i) a low energy band peaked at 0.81 eV, ascribed to band-to-band transitions involving the GaInAs claddings; (ii) a band peaked at 0.92 eV, due to transition of electrons confined in the energy level localized in the InAs layer inside the active region; and (iii) two bands peaked at 1.18 and 1.24 eV, ascribed to transitions between the lowest energy level localized in the ground state injector and two different valence subbands. The evolution of the latter two PL bands with P is reported in Fig. 2(b). The high energy side slope is proportional to $\exp[-E/k_BT_e^j]$, where T_e^g is the electronic temperature of the ground state conduction subband $j=g$. As expected, T_e^g increases with P. The peak energy of each band redshifts with P due to Joule heating. We used this shift as a thermometric property to extract the active region local lattice temperature (T_L) of the device following the procedure described in Refs. 6 and 7.

The increases of T_e^g and T_L with respect to T_H, measured in the active region, are plotted in Fig. 3(a) as a function of P. Below the lasing threshold ($P<2.3$ W), where the total power P is practically coincident with the power dissipated via Joule heating, $\Delta T=T_L-T_H$ increases linearly with P with a slope $R_L=11.5$ K/W, i.e., the thermal resistance. This slope decreases when laser action takes place since an amount of the power comes out optically. T_e^g increases lin-

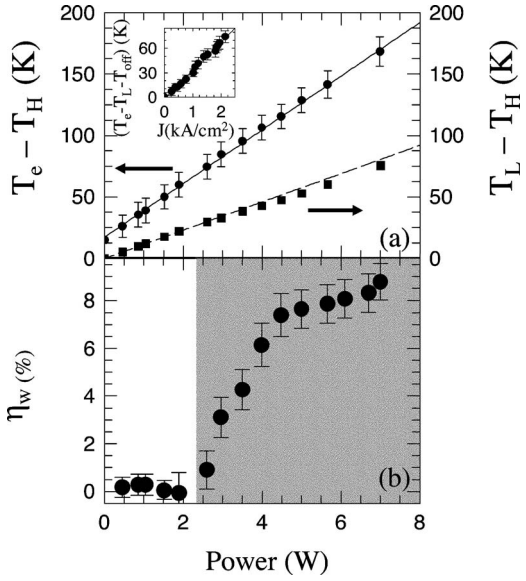

FIG. 3. (a) Electronic and lattice temperatures increases with respect to T_H plotted as a function of the electrical power (P) in the active region of the device. The continuous line is a linear fit to the data. The slope of the dashed line corresponds to the thermal resistance of the device in the region $P<2.4$ W. Inset: electronic temperature increase with respect to T_L as a function of the current density measured at $T_H=60$ K. $T_0=10$ K is the constant temperature shift due to the Kr^+ laser heating. (b) Total wall-plug efficiency plotted as a function of P. The dashed line is a guide for the eye. The shaded area marks the lasing region.

early with P with a slope $R_e=22.0$ K/W larger than R_L. From the measured T_e^g and T_L values, we extracted the electron-lattice coupling constant $\alpha=(T_e^g-T_L)/J=34.8$ K cm^2/kA, which is a measure of the strength of the coupling between electrons and lattice. Low α values correspond to large electron-lattice coupling.[6] The values of $\alpha=29.0$ K cm^2/kA ($\alpha=44.7$ K cm^2/kA) and $\alpha=10.4$ K cm^2/kA have been measured in GaAs/Al_xGa_{1-x}As, with $x=1$ ($x=0.45$) and GaInAs/AlGaAsSb mid-IR QCLs, respectively.[7,12,13] Comparison with the above data indicates a clear correlation between the electron-lattice coupling and the effective band offset. The reduction of the electron-leakage channels associated with the use of high ΔE_C values allows a more efficient cooling of the electronic ensemble.

From the equation $\Delta T/P=(1-\eta_w)\times R_L$, we extracted the total wall-plug efficiency η_w of the investigated device.[14,15] The results are shown in Fig. 3(b). A value $\eta_w=(8.4\pm0.7)\%$ has been extracted at $P=7$ W. This value is a factor $\sim$1.5 higher than the corresponding η_w extracted from the optical measure of P_o [see Fig. 1(c)], thus indicating a collection efficiency $\eta_c\sim0.7$ in the employed optical setup.

To investigate the role of smoother interfaces, induced by interface broadening effects related with the use of InAs/AlAs spikes in the present structure, we have extracted the cross-plane component of the active region thermal conductivity ($k_\perp$). The outcome of a two-dimensional steady state heat dissipation model has been fitted to the experimental data by leaving the anisotropic cross-plane thermal conductivity ($k_\perp$) as the only fitting parameter.[16] We found the value $k_\perp=2.0\pm0.1$ W/(K m), $\sim$1.5 larger than that [$k_\perp=1.4\pm0.1$ W/(K m)] extracted at $T_H=80$ K in GaInAs/AlInAs mid-IR QCLs, from the experimental data of Ref. 16, by using the updated and more reliable function $[-1.1\times10^{-4}\,T^2+0.0425\,T+2.5]$ W/(K m) for the thermal conductivity (k_{InGaAs}) of $Ga_{0.47}In_{0.53}As$ bulk layers,[17] and by scaling k_{InGaAs} by a factor of 1.06 for the $Al_{0.48}In_{0.52}As$ layer.

The parameter $k_\perp$ can be expressed as a function of the bulk resistivities of the materials (R_i) and the average thermal boundary resistance (TBR), which keeps into account the mean contribution of the interface resistivities. The following relation holds $(k_\perp)^{-1}=R_{bulk}+R_{IF}=(\Sigma_i(d_i/d_{tot})R_i+(N/d_{tot})\text{TBR})$, where d_i is the thickness of the GaInAs, AlInAs, InAs, or AlAs layers in the active region, d_{tot} the total active region thickness, and N the total number of interfaces.[7] The bulk resistivity ($R_{bulk}=0.12$ K m/W) has a negligible effect on the thermal conductivity of QCL's active regions. In fact, the latter is mostly determined by the high density of interfaces and hence by the latter term in the above expression for $(k_\perp)^{-1}$. Our results indicate that, in the present case, the use of smoother interfaces with respect to conventional mid-IR GaInAs/AlInAs QCLs reduces the interface resistivity at a value $R_{IF}=0.37$ K m/W, i.e., a factor $\sim$1.5 lower than in standard GaInAs/AlInAs QCLs, and the TBR values in the range $[4.1\times10^{-10}-9.3\times10^{-10}]$ K/W m^2 (Ref. 18) about a factor of 3 lower than in the previous investigated GaInAs/AlInAs QCLs.[16]

CNR-INFM LIT^3 acknowledges partial financial support from Regione Puglia PE-056.

[1] J. S. Yu, A. Evans, S. Slivken, S. R. Darvish, and M. Razeghi, Appl. Phys. Lett. **88**, 251118 (2006).
[2] J. S. Yu, S. Slivken, A. Evans, S. R. Darvish, J. Nguyen, and M. Razeghi, Appl. Phys. Lett. **78**, 1964 (2001).
[3] V. Spagnolo, D. Marano, G. Scamarcio, H. Page, C. Becker, and C. Sirtori, Appl. Phys. Lett. **82**, 4639 (2003).
[4] M. Beck, D. Hofstetter, T. Aellen, J. Faist, U. Oesterle, M. Ilegems, E. Gini, and H. Melchior, Science **295**, 301 (2002).
[5] D. Hofstetter, M. Beck, T. Aellen, J. Faist, U. Oesterle, M. Ilegems, E. Gini, and H. Melchior, Appl. Phys. Lett. **78**, 1964 (2001).
[6] V. Spagnolo, G. Scamarcio, H. Page, and C. Sirtori, Appl. Phys. Lett. **84**, 3690 (2004).
[7] M. S. Vitiello, G. Scamarcio, V. Spagnolo, A. Lops, Q. Yang, C. Manz, W. Bronner, K. Köhler, and J. Wagner, Appl. Phys. Lett. **90**, 121109 (2007).
[8] C. Zhu, Y. Zhang, A. Li, and Z. Tian, J. Appl. Phys. **100**, 053105 (2006).
[9] G. Chen, Phys. Rev. B **57**, 14958 (1998).
[10] D. G. Cahill, W. K. Ford, K. E. Goodson, G. D. Mahan, A. Majumdar, H. J. Maris, R. Merlin, and S. R. Phillpot, J. Appl. Phys. **93**, 793 (2003).
[11] D. A. Carder, L. R. Wilson, R. P. Green, J. W. Cockburn, M. Hopkinson, M. J. Steer, R. Airey, and G. Hill, Appl. Phys. Lett. **82**, 3409 (2003).
[12] V. Spagnolo, G. Scamarcio, W. Schrenk, and G. Strasser, Semicond. Sci. Technol. **19**, 1 (2004).
[13] The conduction band offsets of GaAs/$Al_xGa_{1-x}As$, with $x=1$ ($x=0.45$) and GaInAs/AlGaAsSb QCLs, are 1 eV (0.39 eV) and 1.2 eV, respectively.
[14] J. Vurgaftman and J. R. Meyer, J. Appl. Phys. **99**, 123108 (2006).
[15] M. S. Vitiello, G. Scamarcio, V. Spagnolo, S. S. Dhillon, and C. Sirtori, Appl. Phys. Lett. **90**, 191115 (2007).
[16] A. Lops, V. Spagnolo, and G. Scamarcio, J. Appl. Phys. **100**, 043109 (2006).
[17] G. Zenga, J. E. Bowers, J. M. O. Zide, A. C. Gossard, W. Kim, S. Singer, A. Majumdar, R. Singh, Z. Bian, Y. Zhang, and A. Shakouri, Appl. Phys. Lett. **88**, 113502 (2006).
[18] The thermal boundary resistance values have been calculated in the two limiting conditions. (i) No interface broadening; InAs/InGaAs and AlInAs/AlAs are counted as real interfaces. (ii) Interface broadening takes place; InAs/InGaAs and AlInAs/AlAs are not counted as real interfaces. The influence of InAs and AlAs δ layers on R_{bulk} is negligible.